SUPPORTING MATERIAL

Effects of Hofmeister ions on the α-helical structure of proteins

Alvaro H. Crevenna,[†,*] Nikolaus Naredi-Rainer,[‡,§] Don C. Lamb,[‡,§,¶] Roland Wedlich-Söldner,[†] and Joachim Dzubiella[‖,**,*]

[†] Cellular Dynamics and Cell Patterning, Max Planck Institute of Biochemistry, Martinsried, Germany.

[‡] Physical Chemistry, Department for Chemistry and Biochemistry and Center for Nano Science (CeNS), Ludwig-Maximilians-Universität München, Munich, Germany.
[§] Center for Integrated Protein Science Munich, Munich, Germany.

[¶] Department of Physics, University of Illinois at Urbana-Champaign, Urbana, Illinois.

[‖] Physics Department T37, Technische Universität München, Garching, Germany.

[**] Soft Matter and Functional Materials, Helmholtz-Zentrum Berlin, Berlin, Germany. Physics Department, Humboldt-University Berlin, Berlin, Germany

[*] To whom correspondence should be addressed. E-mail: crevenna@biochem.mpg.de or joachim.dzubiella@helmholtz-berlin.de

SUPPORTING METHODS

CD Spectroscopy

CD experiments were done with a JASCO 715 spectropolarimeter (Jasco, Gross-Umstadt, Germany) and thermal denaturation with a Peltier-thermostat. Peptide concentrations between 30-60 μM were used. The helical fraction was determined assuming the standard linear relationship between spectra at 222 nm and the average peptide α-helicity, i.e. $[\theta]_{222}$ - E_U)/(H - E_U), where H= -44000·(1-(3/N)) is the maximum helical content corrected for finite size effects, N is the number of amino acids, and E_U is the ellipticity of a fully unfolded state (2220) (1). We did not included temperature corrections of the unfolded state signal since all analyses for added salts were done at 273 K.

Molecular dynamics simulation ionic force fields

Briefly, we use the Amber simulation package with the ff03 force-field for the three peptides $A(EAAAK)_2A$, $(AE)_6$ and $(AK)_6$, and the TIP3P model for water. Peptides are blocked by ACE and NME caps at N and C-terminals, respectively. Brute-force MD were performed under NPT conditions with pressure P=1 bar and temperatures T=274 and 300K. REMD was performed using 32 replicas in a T-range between 265 and 520 K each simulated for at least 25 ns. The monoatomic cations and anions in our study are modeled as nonpolarizable Lennard-Jones spheres (2). We simulated each system for 1-2 μs. Secondary structure elements such as the helicity were identified using the DSSP method by Kabsch and Sander (3).

For the monoatomic cations and anions we employed force fields derived by Dang (see for instance (4) and references in (2)) which have been shown to possess reasonable bulk thermodynamic properties (5). Note that these are not the standard Amber ion force fields since they are known to not accurately reproduce crystal and solution properties, see e.g. (6).

For the Lennard-Jones (7) parameters for Gdm^+ we used the Amber ff03 parameters from the arginine side chain for internal consistency. The partial charges for the Gdm^+ atoms have been taken from previous work (8-10) and are +0.64e (C), -0.80e(N), and +0.46(H). ClO_4^- ions were modeled employing parameters developed by Baaden *et al.* (11). All

cross interactions were determined by Lorentz-Berthelot mixing rules as typically employed in the Amber simulations package. 70 to 300 ion pairs were included in the simulation box with box lengths ~3.6-5.0 nm resulting in concentrations between 2.6 and 4.0M. To compare MD-derived peptide configurations to FRET data we additionally simulated Ace-W$(AK)_{14}$CW-Nme in GdmCl, KCl, and $NaClO_4$ for ~1 μs in a dodecahedrical box with a volume of ~150 nm^3 using ~5000 water molecules.

Note that the intra-peptide force field parameters are typically prone to error in reproducing the total amount of secondary structure when benchmarked to experiments or to optimized force field parameterizations, see e.g. (12}). Therefore, we focus on the discussion of effects and qualitative trends with the addition of salt at *fixed* temperature.

m-values from ion partitioning MD simulations

To compare the effects predicted from the experimental partitioning concept and our MD results, we calculated the *m*-value. This is defined as $m = d\Delta G/dc$ [(13) and references therein], where ΔG is the free energy change associated with the folding process. Assuming additivity, the total m-value for the process can be estimated [(13) and Table S1] as:

$$\frac{m}{k_B T} = \sum_i \left(\frac{m_i}{k_B T ASA}\right) (\Delta ASA)_i \,, \quad (1)$$

where m_i are the partial, polar or nonpolar *m*-values which are specific for every salt [(13) and Table S1] and ΔASA is the difference in accessible surface area (*ASA*) between folded and unfolded state ensembles. We extracted the *ASA* for either the polar or nonpolar part of the 'EK'-peptide from salt-free MD simulations. The *ASA* has been estimated using Richard's van der Waals radii (13).

In order to calculate *m*-values from the MD simulations in the presence of salt, we first defined a reaction coordinate $q \in [0,1]$, which measures the normalized root-mean-square distance from a fully helical reference structure (i.e., helicity $h = 1$), averaged over all atoms of the peptide. q can distinguish nicely between folded (q=0.1) and unfolded states ($q \geq 0.6$) as shown previously (14,15). From the equilibrium distribution $P(q)$, we calculated $F(q) = -k_B T \ln P(q)$, the free energy along q. The estimated difference in free energy between folded and unfolded states in the salt-free case is therefore $\Delta F_{\text{salt-free}}$

= $F(0.1)$-$F(\approx 0.6)$ as plotted in supplementary Fig. S1. At a salt concentration c, the salt-induced free energy change is $\Delta G = \Delta F_{\text{salt-free}} - \Delta F_{\text{salt}}$. From this, the m-value can be estimated as $m = d\Delta G/dc = \Delta G/c$, where we assume a linear behavior of ΔG with c. We further assumed an absolute error of $\pm 0.25\ k_BT = \beta^{-1}$ in ΔG, estimated from the maximum statistical fluctuation of $F(q)$ at q=0.1 and q>0.6 , see Fig. S1

m-value correction for a salt bridge

We estimate a salt-bridge contribution $\Delta m_{sb} = m_{corr} - m$ to the ASA-derived m-value by employing the partition coefficient K_{eo} which describes the binding of the salt to the E (ester oxygen) head group. Values of K_{eo} are given in Table S1. The free energy contribution from a E-K (i to i+4) salt bridge has been measured by Scholtz *et al*. (16) and is on the order of $k_BT/2$. Assuming that the interaction is dominated by electrostatics, the total contribution to the free energy of 2 salt bridges is then $G^0_{sb} \sim z_1 z_2 k_B T$, where z_1 and z_2 are the valencies of E and K headgroups, respectively. The non-Columbic contribution to ΔG is then expressed by the decrement of z_1 and by the excess ion coordination $n_{ex} \sim cv(K_{eo}\text{-}1)$ leading to $G_{sb} \sim G^0_{sb}\, cv(K_{eo}\text{-}1)$, where $v \sim 0.5\ nm^3$ is the order of magnitude of the volume of the first solvation shell of the headgroups. With Eq. $\Delta m_{sb} = d\Delta G_{sb}/dc$ and $|z_1| = |z_2| = 1$, it follows that $\Delta m_{sb} \sim G^0_{sb}\, v(K_{eo}\text{-}1) \sim -0.3\,(K_{eo}\text{-}1)\, k_BT\ M^{-1}$.

Ion-peptide backbone coordination in Fig. 2C

The backbone coordination for a given helicity of the EK peptide from the MD simulations, as plotted in Fig 2. *C*, was calculated as follows: we ensemble averaged the number of ions in a volume defined by the sum of the volume of 12 spheres with radius of r_{cut}=0.5 nm around every binding amide atom, i.e., oxygen for the cations and nitrogen for the anions. Only one single value of r_{cut} was taken for all ions to compare absolute numbers of ion hydration in the same volume. This coordination number for a single configuration can then be assigned to the instantaneous helicity and then averaged over all configurations of the same helicity. Error bars have been derived from standard error analysis with error $u^2 = \sigma^2/n$ using the standard deviation σ of the mean coordination with n configurations for a fixed helicity value.

Single molecule experimental setup

To carry out the smFRET experiments, we used a home-build confocal multi-parameter fluorescence setup with pulsed interleaved excitation. For each detected photon all available characteristics are recorded, making it possible to determine the FRET efficiency, fluorescence lifetime of various components, time resolved and steady state anisotropy and stoichiometry; for detailed information see (17). The system is built around a Nikon Ti Eclipse (Nikon, Tokio, Japan) microscope base. Diode lasers were used as picosecond, pulsed excitation sources at 488 nm for donor excitation (LDH-P-C-485, PicoQuant, Berlin) and at 635 nm for acceptor excitation (LDA635, PicoQuant, Berlin). The lasers were combined into a single-mode fiber (AMS Technologies, Planegg, Germany) within a fiber coupling unit (FCU II, PicoQuant, Berlin, Germany), collimated (Schäfter und Kirchhoff, Hamburg, Germany) and focused on the sample by a 60× 1.2NA water immersion objective (Plan Apo VC 60x WI, Nikon, Tokyo, Japan). The average donor and acceptor excitation powers were 100 µW measured before the dichroic mirror (DualLine z488/635, AHF Analysentechnik, Munich, Germany) separating excitation and emission beam paths. The collected fluorescence is focused on a 50µm pinhole with a 60 mm achromatic doublet lens (G322322000, Linos, Göttingen, Germany). A polarizing beamsplitter cube (AHF Analysentechnik) separates the two polarization planes followed by spectral separation in donor and acceptor fluorescence by two dichroic mirrors (BS 650, AHF Analysentechnik, Tübingen, Germany) and four individual emission filters (2x BrightLine HC 525/45 and 2x ET 700/75, AHF Analysentechnik, Tübingen, Germany). Fluorescence is collected by four single photon counting avalanche photodiodes (2x SPQR-14 and 2x SPQR-16, Perkin Elmer, Waltham, Massachusetts) and registered by four individual TCSPC data collection cards (SPC-154, Becker&Hickl, Berlin, Germany). Measurement cards and lasers were synchronized by the laser controller (Sepia 2, Picoquant, Berlin, Germany). The laser pulses were delayed with respect of each other by 18ns, allowing determination of the excitation source by the arrival time of the detected photon using TCSPC. AK_{14} was diluted to 5-20pM concentrations in the desired solvent condition with 0.001% Tween 20 (Pierce) to avoid loss due to unspecific peptide surface adsorption. To correct for background fluorescence, each salt

concentration was measured in the absence of peptide. FRET efficiencies calculated from different experiments were corrected for changes in the index of refraction for each salt type. Samples were measured for 3-5 hours.

Single molecule data analysis

Single-molecule FRET efficiencies were determined using a burst analysis (18). In order to detect the presence of a single molecule via a burst of fluorescence photons, the interphoton times were smoothed using a Lee filter (19). Accordingly, a threshold was set for the maximum allowed time between two photons to be included within the burst. In order to ensure that each molecule contains a donor and acceptor label, the stoichiometry information was used. Stoichiometry values, *S*, for every burst were calculated:

$$S = \frac{I_{DA} - \beta I_{DD} - \alpha I_{AA} + \gamma I_{DD}}{I_{DA} - \beta I_{DD} - \alpha I_{AA} + \gamma I_{DD} + I_{AA} + I_{AD}}$$

where α (= 0.02) is the direct excitation of the donor and β (= 0.02) the donor crosstalk into the acceptor channel. I_{XY} is the number of photons detected after excitation with laser *X* (*D* for donor and *A* for acceptor) in channel *Y*. FRET efficiencies *E* were calculated as:

$$E = \frac{I_{DA} - \beta I_{DD} - \alpha I_{AA}}{I_{DA} - \beta I_{DD} - \alpha I_{AA} + \gamma I_{DD}}$$

Only bursts containing a minimum of 100 photons and a stoichiometry between 0.30 and 0.6 were selected for further analysis. The difference in donor and acceptor quantum yield $\Phi_{D/A}$ and detection efficiency $\eta_{D/A}$ was accounted for by $\gamma = \Phi_A \eta_A / \Phi_D \eta_D$ (0.91 for the measurements presented here). As an additional check on the quality of the performed measurements, lifetime and anisotropy of the fluorescence data were calculated as described in(20). Since time-resolved anisotropy data is available from the multiparameter fluorescence detection measurements, the data was used to estimate the possible values of the orientation factor, κ^2, and hence, the possible error for the Förster radius(21,22). When the time for rotational correlation from protein tumbling is long compared to the fluorescence lifetime ($\theta_{protein} >> \tau$), the anisotropy decays is described by:

$$r(t) = (r_0 - r_\infty)\exp\left(-\frac{t}{\theta_{dye}}\right) + r_\infty$$

where r_∞ is the residual anisotropy, θ_{dye} is the rotational correlation time corresponding to the quick and restricted motion of the dye and r_0 is the fundamental anisotropy. The mobility of the dyes is related to the residual anisotropy of the directly excited donor and acceptor molecules. In contrast, the residual anisotropy of the FRET-mediated fluorescence allows calculation of the angle between the donor and acceptor transition dipoles. Both the time-resolved and steady-state anisotropy measurements of the donor and acceptor fluorophores suggest that an orientation factor of $\kappa^2 = 2/3$ was a reasonable approximation for the calculation of the Förster radius, yielding a value of 51.0 Å for the Atto488-Atto647N FRET pair attached to the $AK_{14}C$ peptide. Measured values of the steady state anisotropy, channel cross-talk and Förster radius were then used for the photon distribution analysis (Fig. S6). Fluorescence lifetimes of the donor and acceptor were also monitored for every measurement to prove that photophysical effects had no influence on quantum yields of the FRET fluorophores. Additionally, *E* was corrected by changes in the Förster radius due to the measured changes of refractive index in the solution with added salt for all three salt types.

Calculation of R_{DA} based on MD-derived structures

In order to compare results from single molecule FRET and MD, the positions of the fluorophores with their linkers need to be accounted for in the MD-derived structures. To do this we first, representative snapshots of specific classes of structures (1. fully helical, 2. fully coiled, 3. highly compact, i.e., minimum radius of gyration) were taken from the MD simulation. Due to the difficulty in achieving equilibrium conditions, we could not choose 'average' states but use instead we chose prominent classes of 3 well-defined, structural states. Second, the end cap Trp residues were removed. The donor dye was located at the N atom of the Ala residue of the N-terminus and the acceptor dye was positioned on the S atom of the Cys residue at the C-terminus. It was done this way to resemble the amino coupling at the N-terminus, and the maleimide labeling at the C-terminus of the $(AK)_{14}$ peptide for experiments. Dye sizes of 7 Å, linker length of 10 Å and linker widths of 4.5 Å were used (23). The accessible volume (AV) of the dyes was then calculated using 'Prior positions' with FRETnpsTools (23). The AV's on the MD-derived structures are displayed on Figure S9 using PyMol (24). A mean position,

$<R_{DA}>_{mp}$, was calculated assuming equal probabilities of the dye position within the AV using 100000 samples and taking into consideration the measured residual anisotropies (0.12 for atto488 and 0.08 for atto647N) and a Förster radius of 51.0 Å. The $<R_{DA}>_{mp}$ was transformed into R^{exp}_{DA} assuming isotropic averaging (25).

SUPPORTING RESULTS

CD spectra of $(GS)_6$

To gain more insight into the issue of $NaClO_4$ affecting the light absorbance of the peptide backbone, we measured the CD spectra of a NH_2-$(GS)_6$-Ace peptide chain in the absence of any salt and at 4 M GdmCl or $NaClO_4$. This chosen sequence does not form any secondary structure (26). Using the 222 nm as helicity criteria, there is a ~5% increase in the helicity in the presence of $NaClO_4$ compared to 2% with GdmCl (Fig. S9). Although a small effect, the trend agrees with the interpretation that $NaClO_4$ modifies the optical properties of the peptide backbone. The effect is likely to be sequence-dependent and may be larger in peptides dominated by alanine groups. In (GS), the polar hydroxyl group of serine, for instance, may compete with $NaClO_4$ in binding to the backbone (26).

Supporting Tables and Figures

Table S1: Ion partitioning coefficents K_i and partial m_i -values per unit *ASA* for polar (p), nonpolar (np) and ester oxygen (eo) compound. m_i/ASA values have units of (nm^{-2} k_BT M^{-1}). Values are taken from (13,27).

	K_p	K_{np}	K_{eo}	m_p/ASA	m_{np}/ASA
KF	1.50	0.57	0.91	-0.46	0.34
KCl	1.63	0.67	0.98	-0.42	0.20
NaCl	1.67	0.63	1.14	-0.42	0.22
GdmCl	1.47	0.97	1.24	-0.37	0.03
$NaClO_4$	2.05	0.79	1.60	-0.70	0.09

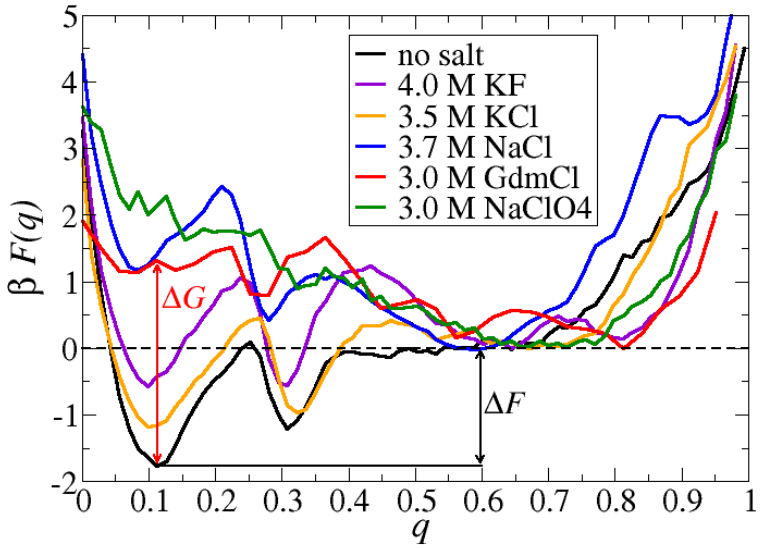

Figure S1: Free energy profile *F*(*q*) along the reaction coordinate *q*. $q \in [0,1]$ is the normalized root-mean square deviation from the perfect helical state. q~0.1 thus corresponds to the full helical state, while $q \geq 0.6$ define unfolded configurations. ΔF is the free energy difference between folded and unfolded states. A specific salt at a concentration c (see legend) specifically shifts this free energy difference by an amount ΔG. From this shift an m-value can be estimated by $m = d\Delta G/dc = \Delta G/c$, where we assume linear behavior of ΔG with c. Given the statistical fluctuations at q=0.6 we assume an error of $\pm 0.25\ k_B T$ in ΔG. β is $(k_B T)^{-1}$.

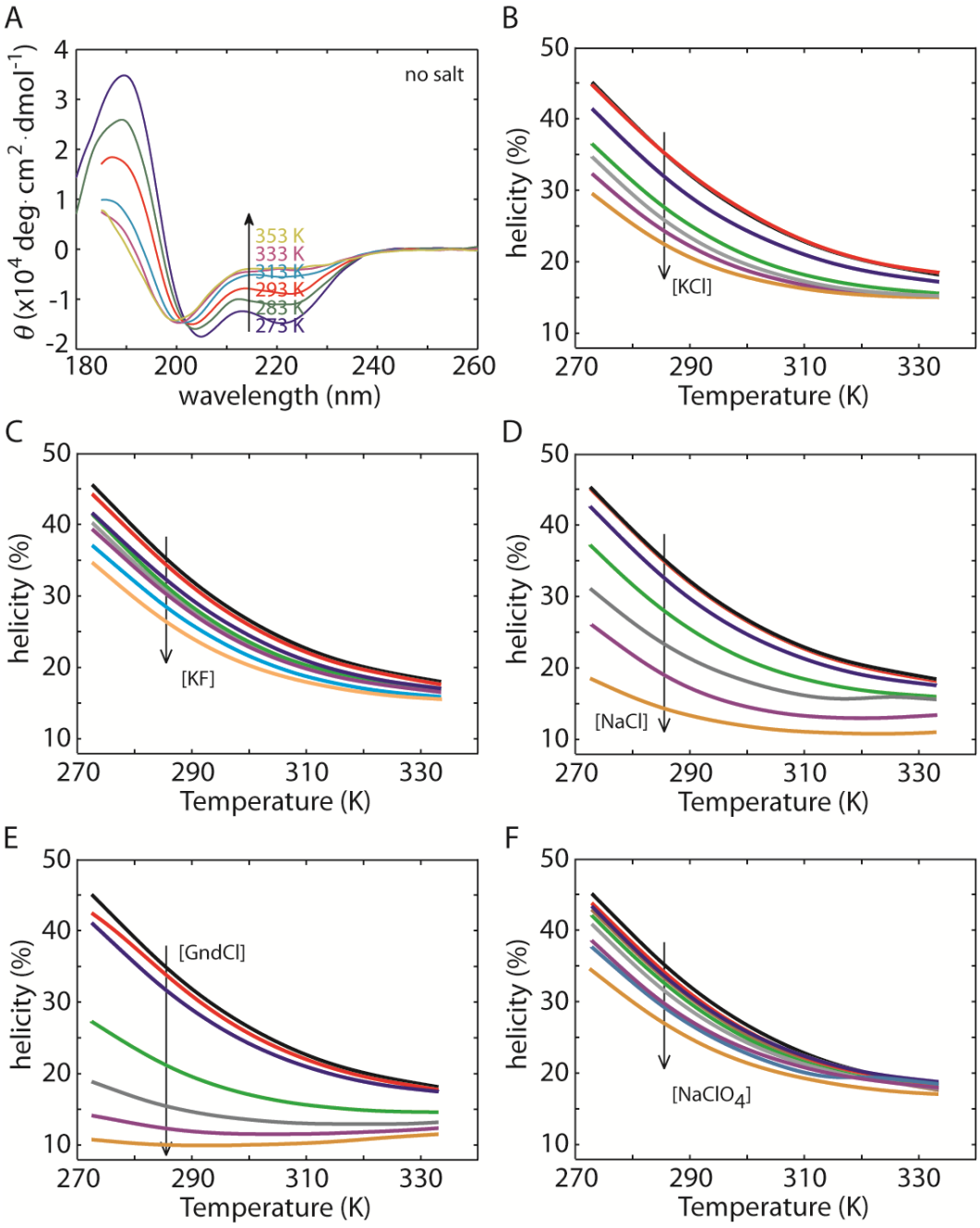

Figure S2. Circular Dichroism 'CD' on the EK peptide. (*A*) CD spectra of the EK peptide at 0 M salt for various temperatures shows the typical double-well signature of an α-helix. A two-state folding transition can be interpreted from the presence of an isobestic point. Thermal denaturation of helicity (calculated from signal at 222 nm) vs. salt concentration for: (*B*) KCl, (*C*) KF, (*D*) NaCl, (*E*) GdmCl, and (*F*) $NaClO_4$.

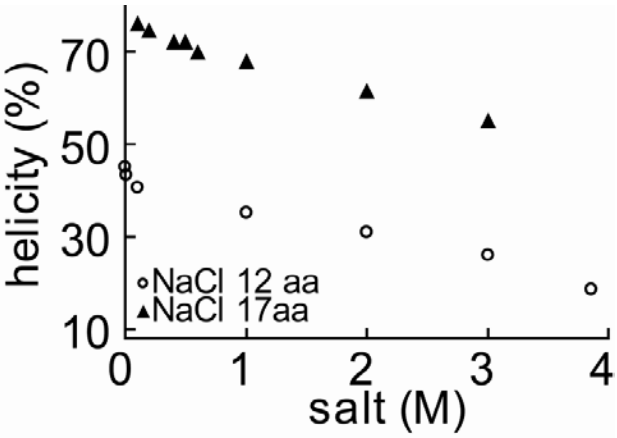

Figure S3. Salt effect versus peptide length. Peptide $A(EAAAK)_NA$ helicity vs [NaCl] for N = 2 (this work) and N = 3 (28). The salt effect is independent of peptide length.

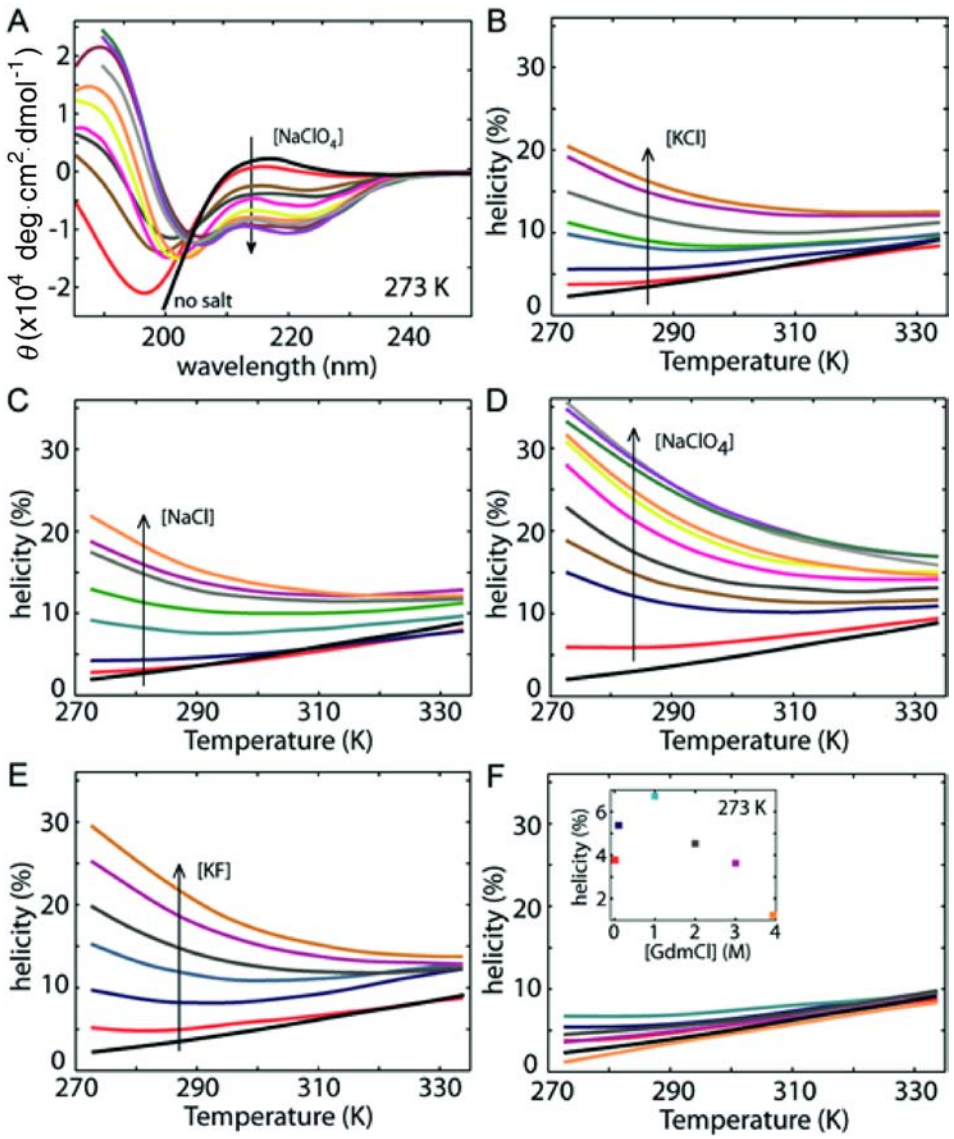

Figure S4. CD on the $(AK)_6$ peptide. (*A*) CD spectra at 0 M salt and vs. $NaClO_4$ concentration. Thermal denaturation of helicity (calculated from signal at 222 nm) vs. salt concentration for: (*B*) KCl, (*C*) NaCl, (*D*) $NaClO_4$, (*E*) KF and (*E*) GdmCl.

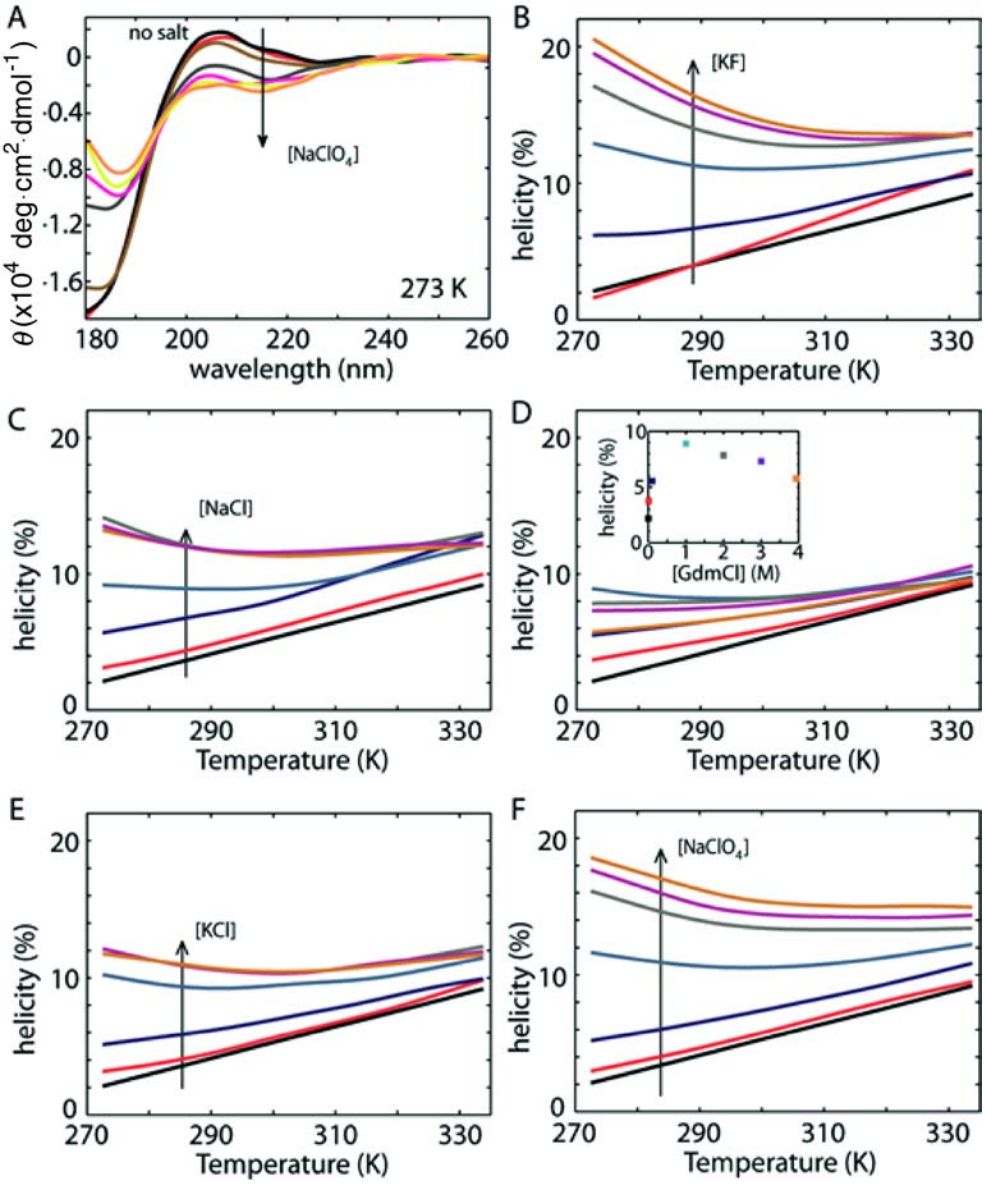

Figure S5. CD on the $(AE)_6$ peptide. (*A*) CD spectra at 0 M salt and vs. $NaClO_4$ concentration. Thermal denaturation of helicity (calculated from signal at 222 nm) vs. salt concentration for: (*B*) KF, (*C*) NaCl, (*D*) GdmCl, (*E*) KCl and (F) $NaClO_4$.

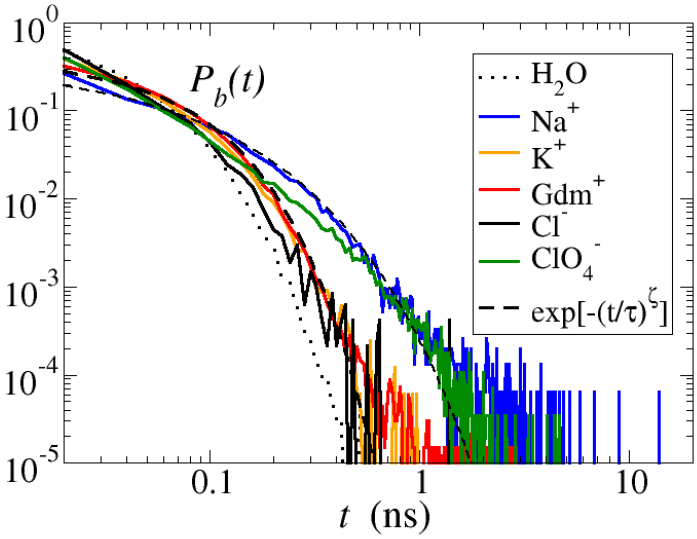

Figure S6. Ion-amide binding kinetics. The binding time distribution $P_b(t)$ of water (O) and ions in the first amide solvation shell. Water, Cl^- K^+ and Gdm^+ ions show a single exponential decay with a time constant τ of ~40 ps. Na^+ and ClO_4^- exhibit anomalous behavior described by a stretched exponential with an exponent ζ of ~0.55 and binding times in the nanosecond regime.

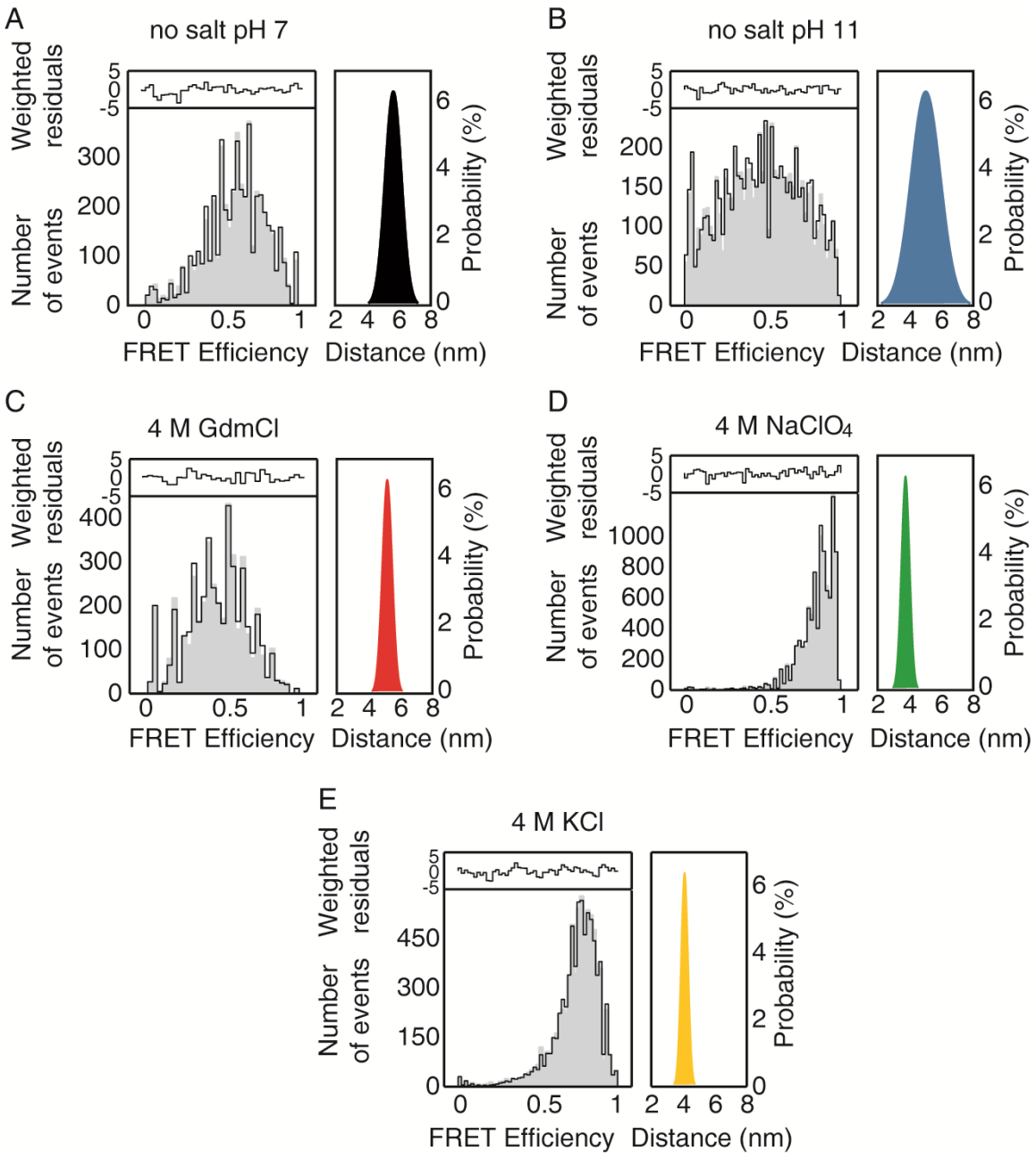

Figure S7. PDA of $(AK)_{14}$ at different salt concentrations. Results from PDA fits (solid lines) for experimental histograms (bars) with weighted residuals are shown for no salt condition at pH 7 (*A*) and pH 11 (*B*); 4 M GdmCl (*C*), 4M $NaClO_4$ (*D*) and 4M KCl (*E*). The estimated gaussian distance probability distribution for each condition is displayed next to it.

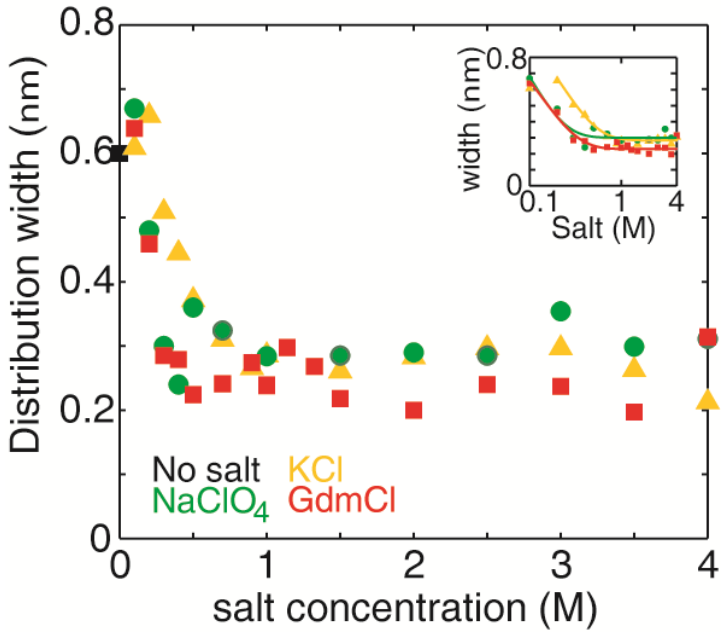

Figure S8. Structural dynamics of $(AK)_{14}$ vs. salt. The residual broadening of the single molecule FRET distribution of R_{DA}, beyond shot noise is plotted as a function of salt concentration. Inset, semilog plot of the data.

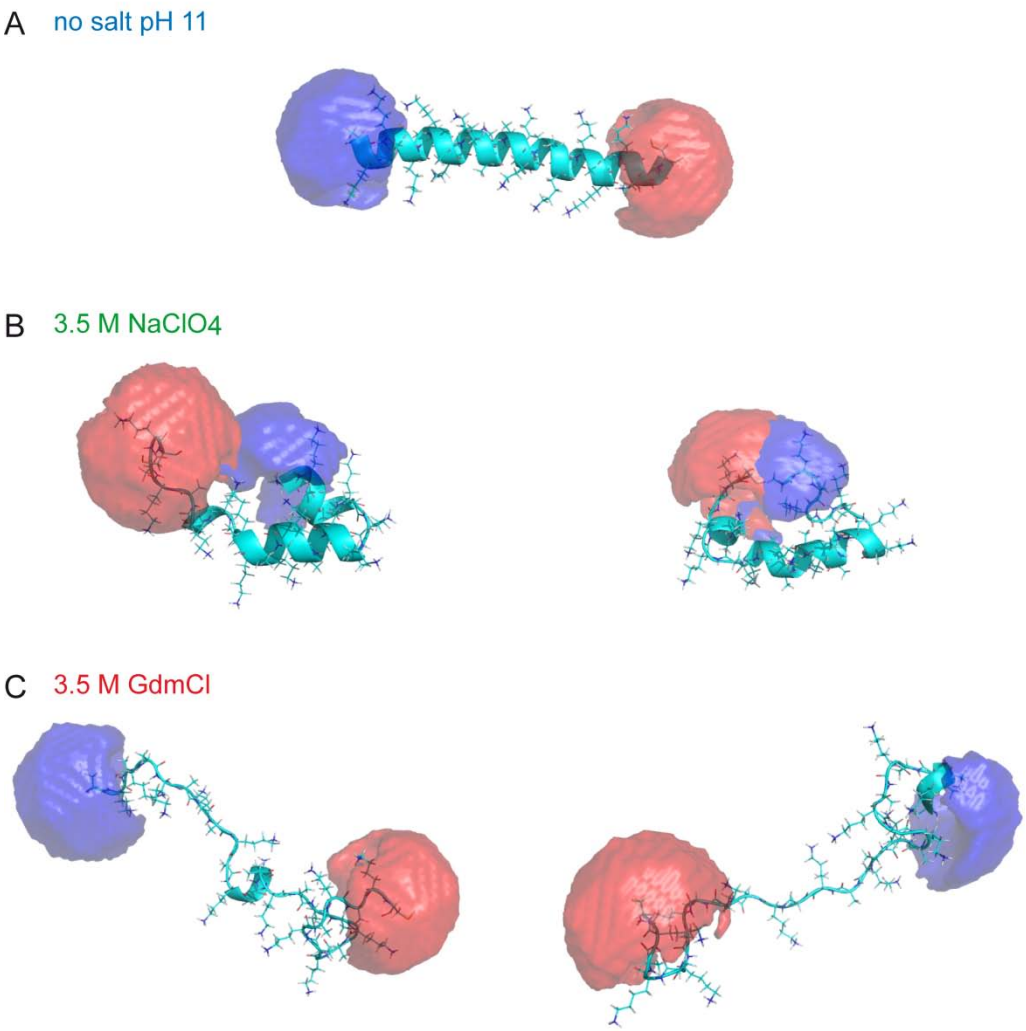

Figure S9. Dye Accessible Volume calculation using MD-derived structures. (*A*) $(AK)_{14}$ no salt pH 11, full α-helical state. Donor (blue) dye attached to N-terminus and acceptor (red) to C-terminus. (*B*) Collapsed states in 3.5M $NaClO_4$. (*C*) Coil-like structures formed at 3.5 M GdmCl.

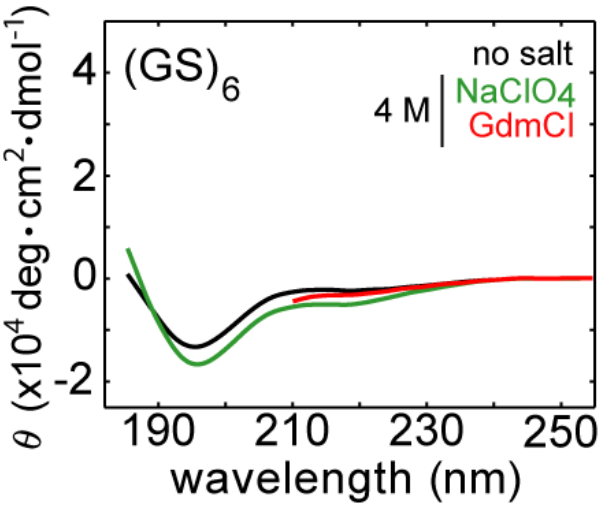

Figure S10. CD spectra of $(GS)_6$ in molar salt. A NH_2-$(GS)_6$-Ace peptide chain in 1mM KAOc pH 7 buffer (no salt), at 4M GdmCl or $NaClO_4$.

SUPPORTING REFERENCES

1. Scholtz, J. M., H. Qian, E. J. York, J. M. Stewart, and R. L. Baldwin. 1991. Parameters of helix-coil transition theory for alanine-based peptides of varying chain lengths in water. Biopolymers 31:1463-1470.

2. Dzubiella, J. 2008. Salt-specific stability and denaturation of a short salt-bridge-forming alpha-helix. J Am Chem Soc 130:14000-14007.

3. Kabsch, W. and C. Sander. 1983. Dictionary of protein secondary structure: pattern recognition of hydrogen-bonded and geometrical features. Biopolymers 22:2577-2637.

4. Dang, L. X. 1995. Mechanism and Thermodynamics of Ion Selectivity in Aqueous Solutions of 18-Crown-6 Ether: A Molecular Dynamics Study. Journal of the American Chemical Society 117:6954-6960.

5. Kalcher, I. and J. Dzubiella. 2009. Structure-thermodynamics relation of electrolyte solutions. The Journal of chemical physics 130:134507.

6. Joung, I. S. and T. E. Cheatham. 2008. Determination of Alkali and Halide Monovalent Ion Parameters for Use in Explicitly Solvated Biomolecular Simulations. The Journal of Physical Chemistry B 112:9020-9041.

7. Fink, A., L. Calciano, Y. Goto, T. Kurotsu, and D. Palleros. 1994. Classification of acid denaturation of proteins - Intermediates and unfolded states. Biochemistry 33:12504-12511.

8. O'Brien, E. P., R. I. Dima, B. Brooks, and D. Thirumalai. 2007. Interactions between hydrophobic and ionic solutes in aqueous guanidinium chloride and urea solutions: lessons for protein denaturation mechanism. J Am Chem Soc 129:7346-7353.

9. Mason, P. E., C. E. Dempsey, L. Vrbka, J. Heyda, J. W. Brady, and P. Jungwirth. 2009. Specificity of ion-protein interactions: complementary and competitive effects of tetrapropylammonium, guanidinium, sulfate, and chloride ions. J Phys Chem B 113:3227-3234.

10. Godawat, R., S. N. Jamadagni, and S. Garde. 2010. Unfolding of hydrophobic polymers in guanidinium chloride solutions. J Phys Chem B 114:2246-2254.

11. Baaden, M., F. Berny, C. Madic, and G. Wipff. 2000. M3+ Lanthanide Cation Solvation by Acetonitrile: The Role of Cation Size, Counterions, and Polarization Effects Investigated by Molecular Dynamics and Quantum Mechanical Simulations. The Journal of Physical Chemistry A 104:7659-7671.

12. Best, R. B. and G. Hummer. 2009. Optimized molecular dynamics force fields applied to the helix-coil transition of polypeptides. The journal of physical chemistry. B 113:9004-9015.

13. Pegram, L. M. and M. T. Record. 2008. Thermodynamic origin of Hofmeister ion effects. Journal of Physical Chemistry B 112:9428-9436.

14. von Hansen, Y., I. Kalcher, and J. Dzubiella. 2010. Ion Specificity in alpha-Helical Folding Kinetics. Journal of Physical Chemistry B 114:13815-13822.

15. Hinczewski, M., Y. von Hansen, J. Dzubiella, and R. R. Netz. 2010. How the diffusivity profile reduces the arbitrariness of protein folding free energies. J Chem Phys 132:245103.

16. Scholtz, J. M., H. Qian, V. H. Robbins, and R. L. Baldwin. 1993. The energetics of ion-pair and hydrogen-bonding interactions in a helical peptide. Biochemistry 32:9668-9676.

17. Kudryavtsev, V., M. Sikor, S. Kalinin, D. Mokranjac, C. A. M. Seidel, and D. C. Lamb. 2012. Combining MFD and PIE for accurate single-pair Förster Resonance Energy Transfer measurements. Chemphyschem.

18. Zander, C., M. Sauer, K. H. Drexhage, D. S. Ko, A. Schulz, J. Wolfrum, L. Brand, C. Eggeling, and C. A. M. Seidel. 1996. Detection and characterization of single molecules in aqueous solution. Applied Physics B: Lasers and Optics 63:517-523.

19. Eggeling, C., S. Berger, L. Brand, J. R. Fries, J. Schaffer, A. Volkmer, and C. A. Seidel. 2001. Data registration and selective single-molecule analysis using multi-parameter fluorescence detection. J Biotechnol 86:163-180.

20. Mapa, K., M. Sikor, V. Kudryavtsev, K. Waegemann, S. Kalinin, C. A. Seidel, W. Neupert, D. C. Lamb, and D. Mokranjac. 2010. The conformational dynamics of the mitochondrial Hsp70 chaperone. Mol Cell 38:89-100.

21. Isaksson, M., N. Norlin, P. O. Westlund, and L. B. Johansson. 2007. On the quantitative molecular analysis of electronic energy transfer within donor-acceptor pairs. Phys Chem Chem Phys 9:1941-1951.

22. Ivanov, V., M. Li, and K. Mizuuchi. 2009. Impact of emission anisotropy on fluorescence spectroscopy and FRET distance measurements. Biophys J 97:922-929.

23. Muschielok, A., J. Andrecka, A. Jawhari, F. Bruckner, P. Cramer, and J. Michaelis. 2008. A nano-positioning system for macromolecular structural analysis. Nat Methods 5:965-971.

24. Schrodinger, LLC. 2010. The PyMOL Molecular Graphics System, Version 1.3r1.

25. Sindbert, S., S. Kalinin, H. Nguyen, A. Kienzler, L. Clima, W. Bannwarth, B. Appel, S. Muller, and C. A. Seidel. 2011. Accurate distance determination of nucleic acids via Forster resonance energy transfer: implications of dye linker length and rigidity. J Am Chem Soc 133:2463-2480.

26. Moglich, A., K. Joder, and T. Kiefhaber. 2006. End-to-end distance distributions and intrachain diffusion constants in unfolded polypeptide chains indicate intramolecular hydrogen bond formation. Proc Natl Acad Sci U S A 103:12394-12399.

27. Pegram, L. M., T. Wendorff, R. Erdmann, I. Shkel, D. Bellissimo, D. J. Felitsky, and M. T. Record. 2010. Why Hofmeister effects of many salts favor protein folding but not DNA helix formation. Proceedings of the National Academy of Sciences. p 7716-7721.

28. Marqusee, S. and R. L. Baldwin. 1987. Helix stabilization by Glu-...Lys+ salt bridges in short peptides of de novo design. Proc Natl Acad Sci U S A 84:8898-8902.